PAPER

CrossMark
click for updates

A new method for high-precision palladium isotope analyses of iron meteorites and other metal samples

Mattias Ek,* Alison C. Hunt and Maria Schönbächler

This paper presents a new method for high precision Pd isotope analyses in iron meteorites. First, Pd is separated from the sample matrix by a novel two-stage anion exchange procedure after which isotopic measurements are carried out using MC-ICP-MS. Analyses of doped standard solutions show that isobaric interference from Ru and Cd can be adequately corrected for Ru/Pd < 0.0005 and Cd/Pd < 0.025. This is frequently achieved using the presented separation method. The purified Pd fraction after ion exchange chromatography is also sufficiently devoid of Ni (Ni/Pd < 0.04), Zr (Zr/Pd < 0.0002) and Zn (Zn/Pd < 0.06) for precise and accurate measurements because these elements produce molecular interference on the masses of the Pd isotopes. An external reproducibility of 1.29 for ε^{102}Pd, 0.22 for ε^{104}Pd, 0.11 for ε^{106}Pd, and 0.27 for ε^{110}Pd is calculated based on the repeated analyses of five independently processed aliquots of the IAB iron meteorite Toluca. The method was verified by the analysis of three metals from IVB iron meteorites and the results show excellent agreement with previous data. The new method enables accurate analysis of all Pd isotopes, and in particular ^{102}Pd, which is of major interest for cosmochemical applications.

1. Introduction

Palladium belongs to the main component elements that are predicted to condense from a gas of solar composition, together with elements such as Fe and Ni. It is therefore considered moderately refractory.[1,2] Palladium is also a highly siderophile element (HSE) and, together with other HSEs, strongly partitions into metal fractions during metal-silicate differentiation, which leads to enrichments in iron meteorites and severe depletion in silicates and the Earth's mantle (*e.g.*, ref. 2–4). Hence, Pd isotope variations could prove a useful and powerful tool for addressing a number of key questions outlined below.

First, in recent years it has become obvious that many elements display small, but well resolvable, nucleosynthetic variations (0.1 per mil range) in meteorites compared to terrestrial samples. Meteorite parent bodies, Mars, and the Earth display unique isotope compositions for a range of elements (*e.g.*, Cr, Ti, Ni, Zr and Mo; *e.g.*, ref. 5–8). These variations stem from the heterogeneous distribution of presolar dust in the solar system carrying highly anomalous isotopic compositions that were synthesised in various stellar environments. They are extremely useful for meteorite provenance studies and provide important constraints on mixing processes in the early solar system. Iron meteorites are thought to represent the core of asteroids that formed, and were subsequently

destroyed, throughout the solar system during the early stages of planet formation.[9] Nucleosynthetic isotope variations in iron meteorites are reported for Ni, Ru, Mo, W and Pd (*e.g.*, ref. 10–17). Palladium is an ideal element to further investigate these variations because it features six stable isotopes that are produced in different stellar environments: one p-process isotope (^{102}Pd), one s-process isotope (^{104}Pd), one predominately r-process isotope (^{110}Pd) and three isotopes (^{105}Pd, ^{106}Pd, and ^{108}Pd) that contain a mixture of s- and r-process components.[18] Accurate measurements of the p-process isotope ^{102}Pd are necessary to differentiate between the s-process and r-process variations that would otherwise be indistinguishable in meteorites. A recent Pd isotope study investigating IVB iron meteorites[16] has reported that Pd nucleosynthetic isotope variations are smaller than those of Ru and Mo, and suggested that this reflects selective destruction of their carrier phases in the solar nebula. However, further high precision Pd isotope analyses of other iron meteorite groups are needed to better constrain this observation.

Moreover, meteorites are exposed to galactic cosmic rays (GCR) during their travel in space. Modelling of GCR exposure for iron meteorites shows that significant isotopic shifts can be induced in many elements, including Pd.[19] Thus, it is important to quantify the GCR effects on Pd isotopes, because Pd isotope variations can be the result of both nucleosynthetic processes and exposure to GCR in space. Isotopic shifts are caused by the capture of secondary neutrons produced by nuclear reactions in meteorites due to irradiation by GCR (*e.g.*, $^{104}_{46}$Pd $+ ^1_0 n \rightarrow ^{105}_{46}$Pd $+ \gamma$). The

Institute of Geochemistry and Petrology, ETH Zürich, Clausiusstrasse 25, 8092 Zürich, Switzerland. E-mail: mattias.ek@erdw.ethz.ch

magnitude of these reactions depends on several factors: (i) isotope-specific properties such as the neutron capture cross section; (ii) meteorite properties such as the matrix composition, original depth of the sample within the meteoroid and time of exposure to GCR; and (iii) epithermal burnout of other elements resulting in the production of unstable isotopes that decay to the isotopes of interest (e.g., $^{103}_{45}Rh + ^{1}_{0}n \rightarrow ^{104}_{45}Rh \rightarrow ^{104}_{46}Pd + ^{0}_{-1}\beta$). All Pd isotopes possess relatively small neutron capture cross sections resulting in small ($\sim<0.2\varepsilon$) isotopic shifts, even for samples with an optimal sample depth and large exposure times. Nevertheless, epithermal burnout of ^{103}Rh can lead to larger ($>1\varepsilon$) isotopic shifts in ^{104}Pd, particularly due to the similar abundance of Rh and Pd in iron meteorites. Epithermal burnout of $^{107,109}Ag$ also occurs but due to the low Ag/Pd ($\sim<1 \times 10^{-4}$) ratio in iron meteorites this reaction is negligible with current precision.

Another motivation to understand and quantify GCR effects in Pd isotopes is the Pd–Ag dating system (e.g. ref. 20 and 21). This chronometer is based on the short-lived isotope ^{107}Pd, which decays to ^{107}Ag with a half-life of 6.5 Ma. Cosmogenic production of the short-lived isotope ^{107}Pd could affect the accuracy of the Pd–Ag dating system.[19,22] High precision Pd isotope analyses, together with the well-established Pt GCR neutron dosimeter, should enable a thorough evaluation of the GCR effects on Pd–Ag chronometry.

Finally, Pd isotopes are a potentially powerful tool to determine the origin of Pd and other HSEs in the Earth. There are two end member scenarios to explain the origin of the HSEs in the Earth's mantle. One proposes that the concentration of HSEs in the mantle reflects the addition of a so-called 'late veneer' to the Earth, post core formation (e.g., ref. 23 and 24). The second scenario states that the Pd (and other HSEs) concentration of the mantle may be achieved during metal-silicate fractionation and core formation in a deep magma ocean, negating the need for a late veneer.[3,25] The terrestrial nucleosynthetic signature relative to meteorites may provide constraints on the source of Pd in the Earth, particularly when correlated with other elements (e.g., Mo[10] and Ru[5,12]).

In order to achieve accurate high precision Pd isotope measurements, it is important that Pd is thoroughly separated from matrix elements, which can cause interference and matrix effects during analysis. For example, Pd isotopes suffer from isobaric interference from Ru and Cd isotopes (Table 1). While Cd abundances are low in iron meteorites, Ru can occur in concentrations similar to Pd (e.g., ref. 26). In particular, high precision measurements of the low abundance ^{102}Pd (1.02%) are hampered due to the high abundance of ^{102}Ru (30%), if Ru is not sufficiently removed prior to mass spectrometry analysis. Molecular interference from matrix elements (i.e., Ni, Zn, and Zr) can also affect the precision and accuracy of the isotopic analyses. Existing procedures for Pd separation from geological matrices are either aimed at abundance determination and do not sufficiently remove matrix elements to enable accurate high precision isotope analyses,[27,28] or fail to efficiently separate Pd from Ru.[16]

Here we present a new method for high precision Pd isotope measurements involving a two-step ion exchange procedure to separate Pd from an iron meteorite matrix. Initial separation of Pd is achieved using a modified version of the ion exchange procedure of Rehkämper and Halliday,[28] described in further detail by Hunt et al.[29] This method allows the collection of both Pd and Pt from the same sample aliquot, enabling direct comparison with the well-established Pt neutron dosimeter. The Pd elution from the first ion exchange column requires further purification before isotopic measurements and a novel procedure to achieve this goal is presented here. First, Ru is removed from the Pd fraction by utilising its volatile nature. Then Pd is separated from the remaining matrix elements using an anion exchange column. This yields a final Pd fraction that is sufficiently devoid of matrix elements, including Ru, to allow for high precision isotopic measurements of all isotopes via multi-collector ICP-MS (MC-ICP-MS). The accuracy of our method was verified by processing one IAB, three IVB iron meteorites and terrestrial standard solutions. Our new analytical method achieves the

Table 1 Collector configuration and isotopic abundances of the isotopes, isobaric interference and major molecular interferents

	101	102	104	105	106	107	108	110	111
Collector configuration									
Cup	L4	L3	L2	L1	C	H1	H2	H3	H4
Resistor (Ω)	10^{12}	10^{11}	10^{11}	10^{11}	10^{11}	10^{11}	10^{11}	10^{11}	10^{12}
Isotope abundances of Pd and isobaric elements (in %; ref. 37)									
Ru	17.06	31.55	18.62						
Pd		1.02	11.14	22.33	27.33		26.46	11.72	
Cd					1.25		0.89	12.49	12.8
Major molecular interferents and their isotopic abundance (in %; ref. 37)									
M^{1}H	^{100}Ru (12.59)	^{101}Ru (17.06)	^{104}Ru (18.62) ^{103}Rh (100)				^{107}Ag (51.83)	^{109}Ag (48.16)	
M^{40}Ar	^{61}Ni (1.14)	^{62}Ni (3.63)	^{64}Ni (0.93) ^{64}Zn (49.17)		^{66}Zn (27.73)	^{68}Zn (4.04)	^{68}Zn (18.45)	^{70}Zn (0.61)	
M^{16}O					^{90}Zr (51.45)	^{91}Zr (11.22)	^{92}Zr (17.15) ^{92}Mo (14.65)	^{94}Zr (17.38) ^{94}Mo (9.19)	^{96}Mo (15.87)

necessary precision and accuracy to enable the thorough evaluation of GCR effects and nucleosynthetic isotope variations in iron meteorites.

2. Methods

2.1 Reagents & materials

Hydrochloric (HCl) and nitric (HNO_3) acids used in this study were twice distilled, while hydrofluoric (HF) acid used was once distilled in dedicated Savillex Teflon stills. The final concentration of these acids after distillation is ~9.6, ~13.9 and ~30 M for HCl, HNO_3 and HF respectively. Merck Suprapur® perchloric ($HClO_4$) acid (70%) and Merck Millipore Bromine Suprapur® (99.9999%) were used without further purification. Reagents were mixed using 18.4 Ω cm^{-1} water supplied by a Millipore™ (Milli-Q©) system. All acids and acid mixtures were titrated before use to ensure accurate molarities. BioRad AG1-X8 resin (200–400 mesh, chloride form) was utilised and batch-cleaned before use.[29]

2.2 Sample digestion

The sample digestion procedure is described by Hunt et al.[29] and a short description of the procedure is given here. Prior to digestion and where necessary, the meteorite samples were sawn using a boron carbide blade operated with ethanol as a cooling fluid. Weathering and fusion crusts were removed using silicon carbide paper. The sample dissolution and ion exchange procedures were performed in laminar flow hoods in a clean laboratory environment. Prior to dissolution, the samples were submerged in ethanol in an ultrasonic bath, followed by leaching in cold 2 M HCl for 5 minutes. The samples were dissolved in a 2 : 1 mixture of concentrated HNO_3 and HCl at 100 °C for 48 hours. They were then dried and re-dissolved in concentrated HCl at 100 °C for 48 hours, which yielded clear solutions of brown colour, indicating that they were fully dissolved.

2.3 Ion-exchange procedure

Palladium was purified in a two-stage ion exchange procedure. The first stage is adapted from Rehkämper and Halliday[28] and described in detail by Hunt et al.[29] After acid digestion, up to 0.3 g of each sample was refluxed at 110 °C in a 2 : 1 mixture of concentrated HCl and HNO_3 (aqua regia) for ~48 hours before being evaporated to dryness. Next the samples were refluxed overnight (~18 hours) in 0.5 M HCl + 10% Br_2–water at 110 °C before being cooled to room temperature. Each aliquot was loaded onto a glass column with 1.25 ml of pre-cleaned BioRad AG1-X8 resin, which was preconditioned with 0.5 M HCl + 10% Br_2–water (Table 2). The loading was followed by the addition of 1 M HCl + 10% Br_2–water, 0.8 M HNO_3 + 10% Br_2–water, and concentrated HCl to elute matrix elements including Fe, Ni and Ru (Table 2). Palladium was eluted from the column in 10 ml of hot (90 °C) 8 M HNO_3 and finally Pt was eluted in 14 ml of 13.5 M HNO_3. The Pd fraction was taken to dryness in preparation for the Ru evaporation stage. The Pt fraction was further processed following the procedure described by Hunt et al.[29]

Ruthenium was removed from the Pd fraction via volatilisation. The Pd fraction from the first ion exchange column was refluxed in 2 ml aqua regia for 48 hours at 110 °C, after which the solution was allowed to cool before 0.3 ml $HClO_4$ was added. The solution was then dried at 210 °C. This step was repeated twice to ensure maximum Ru loss before the second ion exchange column. Tests revealed that evaporation of Ru after the second ion exchange column was much less efficient.

The second ion exchange column was designed to remove matrix elements (notably Fe, Mo, Ru, Ni, and Zr) that remained in the Pd fraction after the first column. In preparation for the second column the Pd fractions were refluxed overnight (~18 hours) in 1 ml 4 M HF before being taken to dryness and again refluxed overnight in 1 ml of 4 M HF. Teflon columns (with an internal diameter of 5 mm) were loaded with 0.5 ml BioRad AG8-X1 resin and rinsed with 10 ml 0.8 M HNO_3, 10 ml concentrated HCl, 10 ml HNO_3, and finally 20 ml 6 M HCl,

Table 2 Palladium ion exchange chromatography

First ion exchange procedure[a]			Second ion exchange procedure		
Resin volume: 1.25 ml AG1-X8			Resin volume: 0.5 ml AG1-X8		
Step	Acid	Volume	Step	Acid	Volume
Cleaning	0.8 M HNO_3	20 ml	Cleaning	0.8 M HNO_3	10 ml
	Concentrated HCl	10 ml		Concentrated HCl	10 ml
	Concentrated HNO_3	25 ml		Concentrated HNO_3	10 ml
	6 M HCl	40 ml		6 M HCl	20 ml
Preconditioning	0.5 M HCl + 10% Br_2[b]	8 ml	Preconditioning	4 M HF	8 ml
Sample loading	0.5 M HCl + 10% Br_2[b]	10 ml	Sample loading	4 M HF	1 ml
Rinse matrix	1 M HCl + 10% Br_2[b]	12 ml	Fe, Ni, Ru	4 M HF	1 ml
Rinse matrix	0.8 M HNO_3 + 10% Br_2[b]	5.5 ml	Ru, Mo	6 M HNO_3	5 ml
Ru	Concentrated HCl	12 ml	Ru, Mo	Concentrated HCl	4 ml
Pd, Ru	8 M HNO_3 (80–90 °C)[c]	10 ml	Pd	Concentrated HCl	4 ml
Pt, Ir	13.5 M HNO_3	14 ml	Pd (Ru)	13.5 M HNO_3	6 ml

[a] From Hunt et al.[29] [b] As bromine saturated water. [c] Loaded in 5 steps of 2 ml.

before being preconditioned with 8 ml 4 M HF (Table 2). The sample was loaded onto the column, and rinsed with 1 ml 4 M HF. Most non-transition metals have very low absorption in HF onto the anion resin and eluted directly.[30,31] This was followed by 5 ml of 6 M HNO_3 to elute remaining Ru and Mo. Subsequently, 4 ml concentrated HCl was added to reduce tailing of Ru into the Pd fraction. Palladium was then eluted in 4 ml concentrated HCl followed by 6 ml 13.5 M HNO_3. The final Pd fraction was generally devoid of elements that potentially form molecular interference (see Section 4.1–2) to enable accurate isotopic determination. This sequence of HCl and HNO_3 minimised the tailing of Pd that occurred otherwise. The Pd cuts were taken to dryness, and then refluxed in 1 ml 5 M HNO_3 at 110 °C overnight before evaporation and preparation for isotopic analyses.

2.4 Yields and procedural blanks

The yield from the first column was typically 70–80%, based on Pd concentrations of iron meteorites from the literature compared to the recovered Pd after the separation procedure. Yields for the second column were often >70%, although yields as low as 50% were also observed. The total yield from both columns was generally >50%. In most cases the final Ru/Pd ratio of samples processed with the method outlined here was <0.0005; however, on rare occasions samples with higher Ru/Pd ratios were observed. These samples were passed through the second column again to reduce their Ru/Pd ratio. Up to 20% of the Ru loaded onto the second ion exchange column can be eluted in the Pd fraction. This highlights the importance of the Ru volatilisation step, where 80–100% of the Ru remaining after the first ion exchange column is lost. Cadmium concentrations are low in iron meteorites (<20 ppb (ref. 32)) and negligible amounts of Cd (Cd/Pd ratios < 0.00001) were determined in the final Pd fraction. Procedural blanks for the ion exchange procedures were routinely collected and were always <1.2 ng g^{-1} sample. No blank correction was therefore necessary since typically >300 ng of Pd was collected for each sample.

3. Mass spectrometry

3.1 Instrumentation and data collection protocols

All measurements were carried out at ETH Zürich using a Thermo Fisher Scientific Neptune *Plus* MC-ICP-MS operated in low resolution mode. Standard H-cones were used and samples were introduced into the plasma using a Cetac Aridus II desolvating system and a nebuliser with an uptake rate of 100 μl min^{-1}. All Pd isotopes were measured simultaneously with 10^{11} Ω resistors, while also monitoring ^{101}Ru and ^{111}Cd using 10^{12} Ω resistors (Table 1). Before each sample/standard measurement, an on-peak baseline (OPB) was measured using a solution containing an acid matrix identical to the subsequent sample/standard. Each OPB and standard/sample measurement consisted of a 30 s electronic baseline measurement followed by collection of 60 integrations (4.7 s each). A peak centre routine was performed immediately prior to each sample/standard analysis. Between measurements, the sample

introduction system was washed with 0.5 M HNO_3 for ~20 min to reduce the background signal to below 1/50th of the original standard/sample signal. The samples were bracketed by measurements of the NIST SRM 3138 Pd standard solution at concentrations that were generally within 15% of the sample. All analyses were carried out in a 0.5 M HNO_3 acid matrix, and solutions were diluted to achieve a signal of 5 to 7 V on ^{105}Pd, typically 100 ng ml^{-1} Pd, when possible. A single measurement typically consumed 1 ml (~100 ng of Pd) of solution and took 10 minutes to complete. The sensitivity of the instrument was between 240 and 340 V ppm^{-1} Pd. The concentrations of matrix elements in the sample solution were checked during each analytical session prior to sample analysis.

3.2 Interference correction and data reduction

Prior to the interference correction, all analyses were background-corrected using the OPB collected before each sample/standard analysis. The analyses were corrected for instrumental mass fractionation (β) using the exponential law,[33] and were internally normalised to ^{108}Pd/^{105}Pd = 1.18899.[34] Isobaric interference from Ru (^{102}Pd and ^{104}Pd) and Cd (^{106}Pd, ^{108}Pd, ^{110}Pd) was corrected using the following procedure. First, the β value for ^{108}Pd/^{105}Pd = 1.18899 was calculated using the measured intensities on mass 105 (^{105}Pd) and mass 108 (^{108}Pd + ^{108}Cd). The contribution to mass 108 from ^{108}Cd was calculated using this β value and the measured intensity on mass 111 (^{111}Cd) together with isotopic abundances of Cd from the study of Rosman *et al.*[35] The calculated ^{108}Cd signal was then subtracted from the measured signal on mass 108 and a new β for ^{108}Pd/^{105}Pd was calculated. This correction procedure was repeated until β converged. The final β value was then used to correct for ^{106}Cd and ^{110}Cd using ^{111}Cd and for interference from ^{102}Ru and ^{104}Ru using ^{101}Ru as an interference monitor together with isotopic abundances from the study of Huang and Masuda.[36] The results are reported relative to ^{105}Pd in epsilon notation (ε), *i.e.*, the deviation of the sample from the average of two bracketing NIST SRM 3138 Pd standards, given in parts per 10 000.

4. Results and discussion

4.1 Isobaric interference

The isobaric interference on Pd isotopes is caused by Ru and Cd isotopes (Table 1). The analysis of NIST SRM 3138 standard solutions doped with Ru and Cd (Table 4 and Fig. 1) demonstrates that Ru/Pd and Cd/Pd ratios of up to 0.001 and 0.025 (respectively) can be accurately corrected within our external reproducibility (discussed in Section 4.3). Above these thresholds the correction breaks down and Ru is under-corrected, yielding positive values for ε^{102}Pd and ε^{104}Pd (Fig. 1A), while Cd is over-corrected, generating negative values, most noticeably on ε^{110}Pd (Fig. 1B).

4.2 Molecular interference

The molecular interference from hydrides (Rh and Ag), argides (Ni and Zn) and oxides (Zr and Mo) can cause spectral

650 | *J. Anal. At. Spectrom.*, 2017, **32**, 647–656

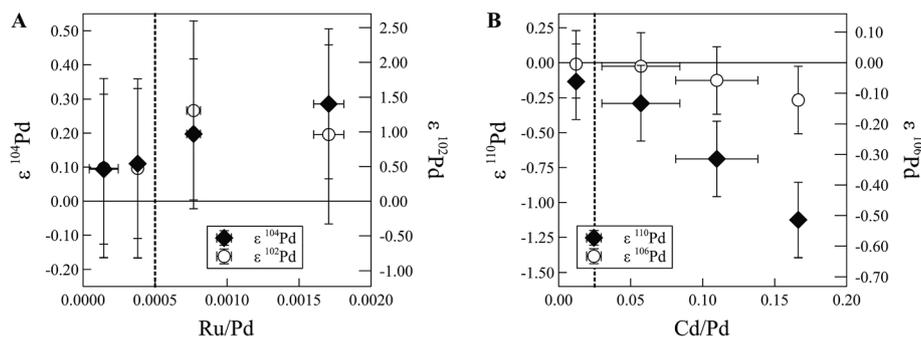This journal is © The Royal Society of Chemistry 2017

Fig. 1 Palladium isotope compositions obtained for a 100 ppb NIST SRM 3138 standard solution doped with Ru (A) and Cd (B) after interference correction. The data points shown are the mean of several analyses. The uncertainties of the isotopic data are reported as our 2 sd external reproducibility derived from Toluca, while, the uncertainty in the elemental ratios is given as the 2 sd of the analysed samples. The vertical dotted line represents the tolerance limit for each element. (A) Accurate corrections for the Ru isobaric interference can be achieved for Ru/Pd below 0.0005. (B) Isobaric interference from Cd can be accurately corrected for up to Cd/Pd ratios of 0.025.

interference on several Pd isotopes (Table 1). The doped Pd standard solutions were analysed in order to constrain the level of these elements that can be tolerated in the final Pd fraction without jeopardizing the accuracy of the data.

Interference from Ni (on ^{101}Ru, ^{102}Pd and ^{104}Pd) and Zn (on ^{104}Pd and ^{106}Pd) argides produces isotopic shifts outside of our external reproducibility at Ni/Pd > 0.04 and Zn/Pd > 0.06 (Table 3 and Fig. 2). The samples processed through our ion exchange procedure rarely yielded Ni/Pd ratios above 0.005 and no sample was above the threshold ratio of 0.04. For Zn/Pd, ratios below 0.06 were consistently achieved after the ion exchange chemistry (Table 3 and Fig. 2B). Our analyses showed that the main source of Zn in our solutions was contamination during the final stages of sample preparation and it is therefore important to monitor the Zn/Pd ratio of samples before every analysis. Our doping tests revealed that production of ^{x}Zr^{16}O depends on the instrumental settings and that ZrO/Zr ratios up to 0.2 can be produced. It is therefore vital to determine ZrO/Zr prior to each analytical session. Typically, the instrument was

calibrated to achieve ZrO/Zr ratios < 0.02. Zirconium/Pd ratios below 0.0002 do not induce isotopic shifts outside of our external reproducibility, when ZrO/Zr = 0.02 (Table 3 and Fig. 2C). Generally, most samples yielded Zr/Pd ratios below 0.00015 after ion exchange chromatography, which is below the threshold if the production of ZrO is minimised. No isotopic shifts were observed for Mo/Pd ratios below 0.34 (Table 3), while Mo/Pd in sample solutions after ion exchange chemistry is typically below 0.005. Additionally, standards with Pt/Pd ratios of up to 0.22 did not introduce resolvable isotopic shifts. This ratio is higher than the typical values obtained for iron meteorites after our ion exchange procedure. Rhenium and Ag can cause both isobaric interference in the form of hydrides and tailing effects on adjacent isotopes (Table 1). However, doping tests at up to Rh/Pd = 0.5 and Ag/Pd = 0.28 show no resolvable isotopic shifts. These levels are well above what is observed in samples (Rh/Pd < 0.01, Ag/Pd < 0.0001) after ion exchange chemistry. The samples with elemental ratios exceeding the stated thresholds (Table 3) were re-processed through the second ion exchange procedure to further purify the samples and achieve accurate results.

4.3 Reproducibility and accuracy

Standard solutions. The long-term average for a 100 ppb NIST SRM 3138 Pd standard solution analysed over the course of three years and 30 analytical sessions is ^{102}Pd/^{105}Pd = 0.045392 ± 5, ^{104}Pd/^{105}Pd = 0.496938 ± 30, ^{106}Pd/^{105}Pd = 1.222805 ± 48, and ^{110}Pd/^{105}Pd = 0.526763 ± 34 (uncertainties are 2σ standard deviations, 2 sd; Fig. 3). The absolute values calculated from these ratios are within 0.03% of those reported by Kelly and Wasserburg,[34] while the IUPAC recommended values[37,38] (after re-normalisation to ^{108}Pd/^{105}Pd = 1.18899) are within 0.22%. The typical reproducibility (2 sd) of the Pd standard solution within an analytical session is 1.19 for ε^{102}Pd, 0.17 for ε^{104}Pd, 0.09 for ε^{106}Pd, and 0.20 for ε^{110}Pd. Three aliquots of NIST SRM 3138 doped with Fe, Ni, and Ru at levels present in iron meteorites were processed through our entire ion exchange procedure separately. Within uncertainty, the means of each aliquot overlap with each other and the mean of the entire data

Table 3 The upper limit of elemental ratios that allow for accurate interference correction

	^{102}Pd	^{104}Pd	^{106}Pd	^{110}Pd
Ru/Pd[a]	0.0005	0.0005		
Cd/Pd[a]			0.1	0.025
Ni/Pd	0.04	0.1		
Zn/Pd		0.06	0.1	
Zr/Pd[b]			0.0002	0.0005
Mo/Pd[c]				>0.34[c]
Rh/Pd[c]		>0.5[c]		
Ag/Pd[c]				>0.28[c]

[a] An interference correction is applied to correct for isobaric interference from Ru and Cd. The correction yields erroneous Pd isotope data if concentrations exceed the indicated limits. [b] This ratio is dependent on the ZrO production during the analyses on the Neptune MC-ICP-MS, which varies from session to session. The limits stated are for a ZrO/Zr value of 2%. [c] No isotopic shifts were detected for this ratio, which is at least 10 times larger than that in sample solutions.
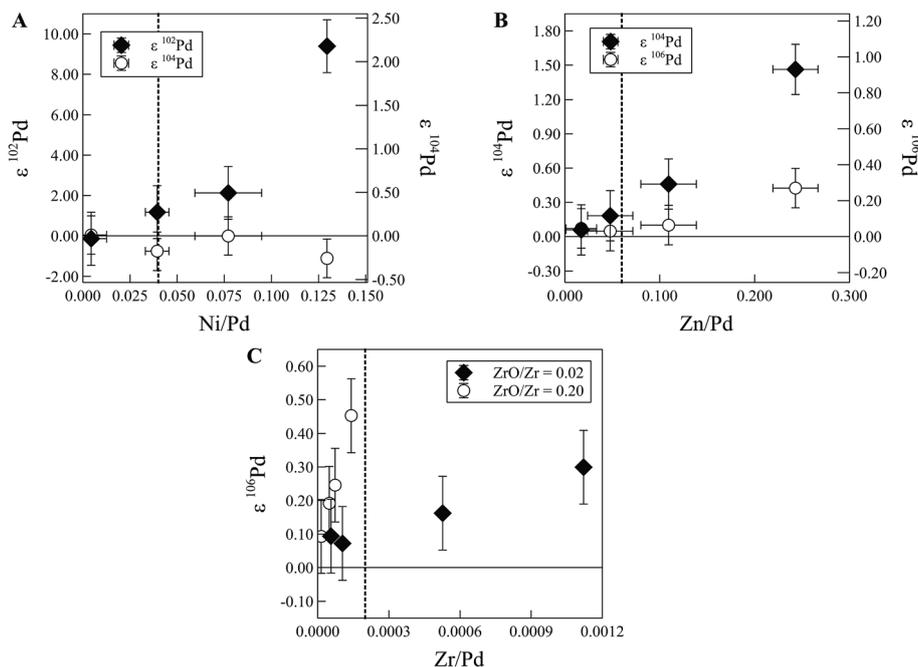
Fig. 2 Palladium isotope compositions of a 100 ppb NIST SRM 3138 Pd standard solution doped with varying amounts of Ni (A), Zn (B) and Zr (C). The data points for (A and B) are the mean of several analyses, while the data points in (C) are single analyses. The uncertainties of the isotopic data are reported as the 2 sd of our external reproducibility (derived from Toluca), while, the uncertainty in the elemental ratios is given as the 2 sd of the analysed samples. The vertical dotted lines illustrate the maximum amount tolerated for each element. Ratios below (A) Ni/Pd = 0.04, (B) Zn/Pd = 0.06, and (C) Zr/Pd = 0.0002 (for ZrO/Zr = 0.02) do not cause any resolvable isotopic shifts outside of our external reproducibility.
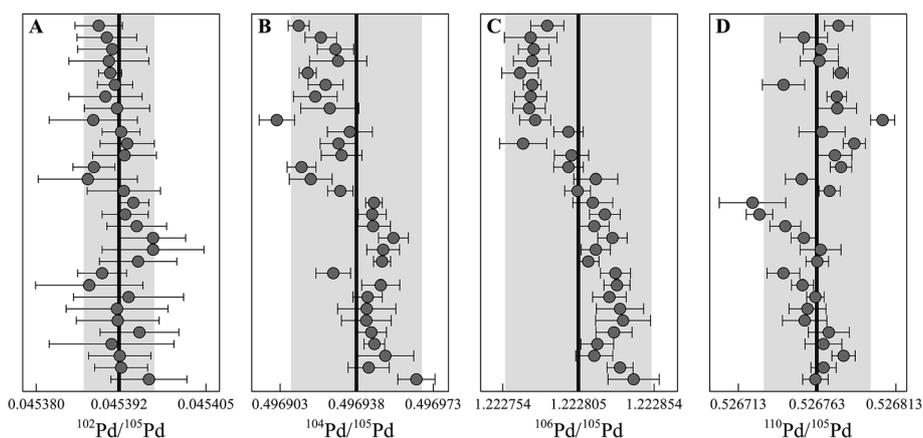

Fig. 3 The average Pd isotope ratios of the NIST SRM 3138 Pd standard, internally normalised to $^{108}Pd/^{105}Pd$, for ~100 ppb solutions obtained over 30 analytical sessions during the course of three years. The uncertainties represent the 2 sd within-session reproducibility, while the grey band represents the 2 sd long-term reproducibility based on all the session averages.

set yielded no resolvable differences from the unprocessed bracketing standard (Table 4). This verifies the accuracy of our data and demonstrates that (i) isotope fractionation did not occur during the ion exchange procedure beyond that corrected for using the internal normalisation procedure, and (ii) that all isobaric and molecular interference was either accurately corrected for or absent in the analysed fractions.

IAB iron meteorites. Repeated measurements of five independently processed sample aliquots of the IAB iron meteorite Toluca (ETH meteorite collection) were performed to assess the

sample reproducibility of our method for a sample with a natural matrix. The means of all aliquots overlap within uncertainty for all isotopes (Table 5 and Fig. 4), which indicates that there is no isotopic difference between the aliquots. The reproducibility calculated based on our entire Toluca data set (n = 20; 2 sd) is 1.29 for $\varepsilon^{102}Pd$, 0.22 for $\varepsilon^{104}Pd$, 0.11 for $\varepsilon^{106}Pd$, and 0.27 for $\varepsilon^{110}Pd$ (Fig. 4). These uncertainties are similar or slightly higher compared to those calculated from the doped synthetic solutions (Table 4), which we attribute to the more complex matrix of the natural samples. Since they were

Table 4 Three aliquots of NIST SRM 3138 Pd standard, doped with an iron meteorite matrix, independently processed through the new analytical procedure

Sample name[a]	Ru/Pd	ε^{102}Pd	2 se[b]	ε^{104}Pd	2 se[b]	ε^{106}Pd	2 se[b]	ε^{110}Pd	2 se[b]
NIST SRM 3138 Pd 1a	0.00013	−0.18	0.37	−0.01	0.11	−0.03	0.06	−0.03	0.13
NIST SRM 3138 Pd 1b	0.00013	−0.25	0.40	0.06	0.12	−0.01	0.08	−0.03	0.11
NIST SRM 3138 Pd 1c	0.00012	0.55	0.34	0.03	0.11	0.03	0.08	0.07	0.11
NIST SRM 3138 Pd 1d	0.00015	1.16	0.41	−0.07	0.12	0.13	0.08	0.01	0.13
NIST SRM 3138 Pd 1e	0.00016	−1.07	0.36	−0.03	0.12	−0.03	0.07	−0.07	0.14
NIST SRM 3138 Pd 1f	0.00018	−0.26	0.43	−0.10	0.12	−0.03	0.08	−0.12	0.14
NIST SRM 3138 Pd 1 mean ($n = 6$)	**0.00014**	**−0.01**	**0.63**	**−0.02**	**0.05**	**0.01**	**0.05**	**−0.03**	**0.05**
NIST SRM 3138 Pd 2a	0.00005	1.58	0.35	0.12	0.13	−0.06	0.08	−0.09	0.11
NIST SRM 3138 Pd 2b	0.00005	0.40	0.55	−0.08	0.13	0.07	0.07	0.03	0.13
NIST SRM 3138 Pd 2c	0.00004	0.65	0.40	0.01	0.12	0.11	0.06	0.13	0.16
NIST SRM 3138 Pd 2d	0.00003	1.25	0.42	0.00	0.12	−0.03	0.08	−0.05	0.15
NIST SRM 3138 Pd 2e	0.00003	−0.37	0.36	0.02	0.16	−0.03	0.09	0.03	0.15
NIST SRM 3138 Pd 2 mean ($n = 5$)	**0.00004**	**0.70**	**0.68**	**0.01**	**0.06**	**0.01**	**0.06**	**0.01**	**0.08**
NIST SRM 3138 Pd 3a	0.00010	0.18	0.33	0.04	0.14	0.03	0.06	0.09	0.12
NIST SRM 3138 Pd 3b	0.00011	0.38	0.51	0.02	0.14	0.03	0.08	0.04	0.15
NIST SRM 3138 Pd 3c	0.00009	0.92	0.48	−0.10	0.12	−0.06	0.07	0.13	0.15
NIST SRM 3138 Pd 3d	0.00010	0.62	0.39	0.05	0.13	−0.07	0.09	0.17	0.12
NIST SRM 3138 Pd 3 mean ($n = 4$)	**0.00010**	**0.53**	**0.32**	**0.00**	**0.07**	**−0.02**	**0.05**	**0.11**	**0.06**
NIST SRM 3138 Pd mean[c] ($n = 15$)		**0.37**	**1.42**	**0.00**	**0.12**	**0.00**	**0.12**	**0.02**	**0.17**

[a] Number after the sample name denotes sample aliquot and the letter indicates duplicate analyses of the sample aliquot. Each aliquot was processed separately through the entire separation procedure. [b] Uncertainties in the individual analyses are reported as the 2σ standard errors (2 se) on the mean of the individual ratios obtained in a single analysis, while uncertainty in the mean of each aliquot is reported as the 2 se of the analyses. For means calculated based on analyses from multiple aliquots the uncertainty is reported as 2 sd. [c] Mean calculated based on the entire data set of that sample.

obtained on natural samples, we consider their uncertainty as a better approximation of the overall sample reproducibility and applied it for the inference tests described in Section 4.1 and 4.2.

IVB iron meteorites. Three IVB iron meteorites (Hoba, BM 19030, 976, loaned by the Natural History Museum London; Santa Clara and Tawallah Valley, ETH collection), which were analysed in a previous Pd study,[16] were also processed to test the reproducibility and accuracy of our method. The ε^{106}Pd values of these samples are all identical to the terrestrial value, within uncertainty (Fig. 5C and Table 5). All IVB meteorites show a resolved ε^{104}Pd deficit relative to the Earth (Fig. 5B) and well-resolved excesses of a similar magnitude in ε^{110}Pd ($\sim$+0.6; Fig. 5D). Santa Clara is within uncertainty of the terrestrial value for ε^{102}Pd while Hoba shows a very small negative offset compared to the terrestrial value (Fig. 5A). Tawallah Valley shows a resolvable positive offset for ε^{102}Pd that is not within uncertainty of the other two samples; however, this sample has a high Ni/Pd ratio ($\sim$0.03) that could affect accuracy at the given precision. The ε^{104}Pd, ε^{106}Pd and ε^{110}Pd values are in excellent agreement with those reported by Mayer et al.[16] (Fig. 5) for the same meteorites, verifying the accuracy of our method. Mayer et al.[16] observe large isotopic offsets for ε^{102}Pd and state that they reflect inaccurate correction of the isobaric ^{102}Ru interference due to high Ru/Pd ratios in their sample solutions after the ion exchange procedure. Our data confirm their conclusion, because, in contrast to the previous work, our new analytical procedure yields low Ru/Pd ratios that are below the threshold at which the interference correction breaks down (Tables 3–5). The IVB iron meteorites contain relatively high amounts of Ru

(Ru/Pd > 2 (ref. 26)) and this also verifies the ability of our method to separate and/or correct for Ru interference, even for samples with high Ru/Pd ratios.

4.4 Cosmochemical implication for IAB and IVB iron meteorites

The well-resolved deficits in ε^{104}Pd ($\sim$−0.2) and excess in ε^{110}Pd (+0.6) for the three IVB meteorites most likely reflect the presence of a nucleosynthetic s-process deficit/r-process excess (^{104}Pd is an s-process isotope and ^{110}Pd is an r-process isotope) coupled with the effects of GCR. Both GCR and an s-process deficit/r-process excess will increase the ε^{110}Pd ratio of a sample. The three IVB meteorite samples share a very similar GCR exposure history,[16] which resulted in this relatively constant positive offset. Similarly, the negative offsets in ε^{104}Pd (Fig. 5) are likely generated by a combination of GCR and nucleosynthetic effects, as discussed by Mayer et al.[16] Studies of p-process isotopes of other elements such as Mo[10] and Ru[12] allow an s-process deficit to be resolved from an r-process excess; however, the precision of our ε^{102}Pd data is not sufficient to distinguish between an s-process deficit and an r-process excess without further investigation. Thus a more thorough evaluation of the GCR effects in our samples is needed to elucidate the details. Combining Pd with Pt isotope analyses obtained on the same sample aliquots will act as a neutron dosimeter, and allow for a decisive statement about the respective magnitude of the nucleosynthetic and GCR effects.

In contrast, the Pd isotope analyses of the IAB meteorite Toluca yield identical isotope compositions to the terrestrial

Table 5 The Pd isotopic composition of 5 aliquots of Toluca and a single aliquot of Tawallah Valley, Santa Clara, and Hoba processed using the new analytical procedure

Sample name[a]	Ru/Pd	ε^{102}Pd	2 se[b]	ε^{104}Pd	2 se[b]	ε^{106}Pd	2 se[b]	ε^{110}Pd	2 se[b]
Toluca 1a	0.00002	−0.64	0.49	−0.17	0.16	−0.02	0.08	0.13	0.18
Toluca 1b	0.00001	0.34	0.37	0.03	0.10	−0.07	0.07	−0.23	0.15
Toluca 1c	0.00001	1.57	0.41	0.31	0.15	0.00	0.08	−0.20	0.14
Toluca 1d	0.00071	−0.17	0.50	−0.03	0.15	0.06	0.09	−0.14	0.15
Toluca 1 (IAB) mean ($n = 4$)	**0.00019**	**0.28**	**0.95**	**0.04**	**0.20**	**−0.01**	**0.06**	**−0.11**	**0.17**
Toluca 2a	0.00003	0.67	0.35	−0.04	0.11	−0.03	0.07	−0.12	0.14
Toluca 2b	0.00002	−0.55	0.40	−0.11	0.12	0.03	0.06	−0.01	0.14
Toluca 2c	0.00002	0.63	0.51	−0.16	0.19	−0.04	0.09	−0.20	0.14
Toluca 2d	0.00003	−0.35	0.54	−0.06	0.13	−0.11	0.09	0.02	0.14
Toluca 2 (IAB) mean ($n = 4$)	**0.00003**	**0.10**	**0.65**	**−0.09**	**0.11**	**−0.04**	**0.06**	**−0.08**	**0.14**
Toluca 3a	0.00022	0.31	0.36	−0.06	0.14	−0.02	0.07	−0.25	0.13
Toluca 3b	0.00022	0.54	0.36	−0.02	0.11	−0.03	0.07	−0.05	0.12
Toluca 3c	0.00050	1.17	0.41	0.08	0.10	−0.04	0.07	−0.04	0.12
Toluca 3d	0.00051	−0.08	0.42	−0.04	0.14	−0.02	0.07	0.06	0.14
Toluca 3 (IAB) mean ($n = 4$)	**0.00036**	**0.49**	**0.65**	**−0.01**	**0.11**	**−0.03**	**0.06**	**−0.07**	**0.14**
Toluca 4a	0.00000	−0.59	0.29	−0.23	0.11	−0.03	0.06	0.02	0.13
Toluca 4b	0.00000	−0.56	0.39	−0.08	0.11	−0.01	0.08	−0.05	0.13
Toluca 4c	0.00000	0.19	0.47	−0.03	0.14	0.02	0.07	0.29	0.14
Toluca 4d	0.00000	1.19	0.40	0.06	0.13	−0.04	0.08	−0.02	0.14
Toluca 4 (IAB) mean ($n = 4$)	**0.00000**	**0.06**	**0.83**	**−0.07**	**0.12**	**−0.02**	**0.06**	**0.06**	**0.17**
Toluca 5a	0.00006	0.78	0.39	0.01	0.14	0.01	0.06	−0.15	0.13
Toluca 5b	0.00006	0.70	0.39	0.00	0.15	0.15	0.07	−0.09	0.13
Toluca 5c	0.00007	0.20	0.43	0.02	0.13	0.07	0.08	0.06	0.14
Toluca 5d	0.00007	−0.13	0.38	−0.02	0.14	−0.03	0.07	0.13	0.15
Toluca 5 (IAB) mean ($n = 4$)	**0.00007**	**0.39**	**0.65**	**0.00**	**0.11**	**0.05**	**0.08**	**−0.01**	**0.14**
Toluca (IAB) mean[c] ($n = 20$)		**0.26**	**1.29**	**−0.03**	**0.22**	**−0.01**	**0.11**	**−0.04**	**0.27**
Tawallah Valley 1a	0.00020	−0.75	0.49	−0.25	0.17	0.04	0.10	0.58	0.20
Tawallah Valley 1b	0.00017	0.65	0.53	−0.49	0.14	−0.03	0.08	0.55	0.16
Tawallah Valley 1c	0.00017	1.92	0.52	−0.49	0.13	−0.01	0.09	0.64	0.17
Tawallah Valley 1d	0.00012	2.00	0.42	−0.47	0.12	−0.13	0.08	0.49	0.15
Tawallah Valley 1e	0.00013	0.81	0.75	−0.50	0.14	−0.08	0.09	0.61	0.16
Tawallah Valley 1f	0.00015	2.11	0.44	−0.21	0.17	−0.12	0.09	0.50	0.16
Tawallah Valley 1g	0.00014	1.31	0.51	−0.21	0.13	−0.11	0.08	0.67	0.15
Tawallah Valley 1h	0.00015	−0.30	0.47	−0.30	0.16	−0.06	0.07	0.53	0.14
Tawallah Valley 1i	0.00015	0.97	0.40	−0.16	0.10	0.07	0.08	0.56	0.13
Tawallah Valley (IVB) mean ($n = 9$)	**0.00015**	**0.97[d]**	**0.67**	**−0.34**	**0.10**	**−0.05**	**0.05**	**0.57**	**0.09**
Santa Clara 1a	0.00012	−0.92	0.50	−0.25	0.17	0.00	0.11	0.55	0.14
Santa Clara 1b	0.00009	−1.63	0.58	−0.03	0.17	0.02	0.10	0.44	0.18
Santa Clara 1c	0.00008	0.32	0.40	−0.11	0.11	0.01	0.07	0.62	0.11
Santa Clara 1d	0.00008	−0.07	0.42	0.00	0.13	−0.01	0.07	0.83	0.14
Santa Clara 1e	0.00008	0.30	0.62	0.05	0.12	−0.07	0.07	0.81	0.14
Santa Clara 1f	0.00008	−0.12	0.43	−0.10	0.13	0.02	0.07	0.76	0.16
Santa Clara 1g	0.00008	−0.09	0.38	−0.12	0.12	0.02	0.08	0.47	0.15
Santa Clara 1h	0.00009	−0.25	0.36	0.02	0.12	0.08	0.07	0.47	0.13
Santa Clara (IVB) mean ($n = 8$)	**0.00009**	**−0.31**	**0.47**	**−0.07**	**0.08**	**0.01**	**0.04**	**0.62**	**0.11**
Hoba 1a	0.00004	−1.17	0.41	−0.32	0.12	−0.02	0.07	0.38	0.15
Hoba 1b	0.00004	−0.68	0.42	−0.37	0.12	−0.04	0.08	0.46	0.17
Hoba 1c	0.00004	−0.35	0.42	−0.21	0.16	−0.01	0.09	0.39	0.14
Hoba 1d	0.00004	−0.77	0.42	−0.16	0.15	−0.06	0.08	0.24	0.17
Hoba (IVB) mean, ($n = 4$)	**0.00004**	**−0.74**	**0.65**	**−0.27**	**0.11**	**−0.03**	**0.06**	**0.37**	**0.14**

[a] Number after the sample name denotes sample aliquot and the letter indicates duplicate analyses of the sample aliquot. Each aliquot was processed separately through the entire separation procedure. [b] Uncertainties in the individual analyses are reported as the 2σ standard errors (2 se) on the mean of the individual ratios obtained in a single analysis. The 2 se uncertainty in the mean of an aliquot is calculated as the 2 sd of the aliquot or the 2 sd of the Toluca mean (whichever is larger) divided by the square root of n. For means calculated based on analyses from multiple aliquots the uncertainty is reported as the 2 sd. [c] Mean calculated based on the entire data set of that sample. [d] Tawallah Valley has a high Ni/Pd ratio (∼0.03) which may affect the accuracy of the ε^{102}Pd data.

standard. This indicates that our Toluca sample was not strongly exposed to GCR. This is in agreement with a study of the GCR exposure of the Toluca 1 aliquot by Hunt et al.[39] using Pt isotopes. Moreover, the data also testify to the absence of nucleosynthetic variations in IAB meteorites, which confirms results from other elements, such as Mo[10] and Ru.[12]
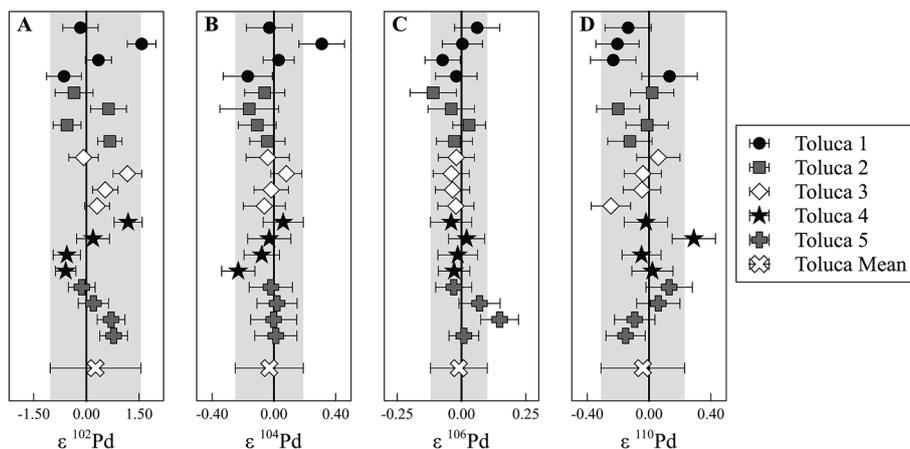
Fig. 4 Repeated measurements of five independently processed aliquots of the IAB iron meteorite Toluca for ε^{102}Pd (A), ε^{104}Pd (B), ε^{106}Pd (C) and ε^{110}Pd (D). The shaded area and the uncertainty of Toluca mean represent the 2 sd of the overall mean of Toluca, also taken as our external reproducibility. The uncertainty of the individual measurements of the five aliquots represents the 2 se internal uncertainty of each analysis. The overall mean for Toluca is within uncertainty of the terrestrial composition for all isotopes.
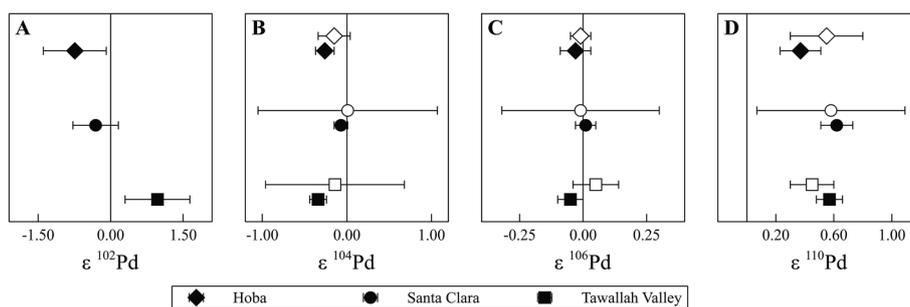
Fig. 5 The mean Pd isotope compositions of three IVB iron meteorites (Hoba, Santa Clara, and Tawallah Valley) from this study (filled symbols) compared to those reported by Mayer et al.[16] (open symbols). The uncertainties in our values are given as the 2 se of several analyses, while the uncertainty of the data from Mayer et al.[16] represents the 2 se internal uncertainty. The values from the two studies are in excellent agreement for ε^{104}Pd, ε^{106}Pd and ε^{110}Pd. The ε^{102}Pd values from Mayer et al.[16] are not shown because of large Ru interference.

5. Conclusions

We present a new analytical method for separating Pd from iron meteorites for high precision isotope analysis. Our separation procedure yields sample solutions with minimal amounts of Ru and other elements (e.g., Zn and Zr) that produce interference during mass spectrometry. Following initial Pd separation from the iron meteorite matrix using an anion exchange resin, Ru is volatilised and removed from the sample. A second anion exchange column is employed to remove remaining matrix elements including Ru. The new analytical procedure yields an external reproducibility (2 sd) of 1.29 for ε^{102}Pd, 0.22 for ε^{104}Pd, 0.11 for ε^{106}Pd, and 0.27 for ε^{110}Pd based on repeated analyses of five independently processed aliquots of the IAB iron meteorite Toluca. The method was also successfully applied to three IVB iron meteorites (Tawallah Valley, Santa Clara, and Hoba) and our Pd isotope data are in excellent agreement with those reported by Mayer et al.[16] for the same meteorites. Our new procedure achieves separation of Ru from Pd to a high degree, which allows for the accurate determination of ε^{102}Pd.

The Pd isotope compositions of the three IVB iron meteorites are consistent with the presence of a nucleosynthetic s-process deficit/r-process excess, while the data for Toluca indicate that these effects are absent in IAB meteorites. Further work, however, is required for a thorough evaluation of GCR effects in IAB and IVB iron meteorites.

Acknowledgements

References

1 K. Lodders, Astrophys. J., 2003, 591, 1220–1247.
2 H. Palme and H. S. C. O'Neill, Treatise Geochem., 2014, 2, 1–38.

3 U. Mann, D. J. Frost, D. C. Rubie, H. Becker and A. Audétat, *Geochim. Cosmochim. Acta*, 2012, **84**, 593–613.

4 K. Righter, *Earth Planet. Sci. Lett.*, 2011, **304**, 158–167.

5 W. Akram, M. Schönbächler, S. Bisterzo and R. Gallino, *Geochim. Cosmochim. Acta*, 2015, **165**, 484–500.

6 A. Trinquier, T. Elliott, D. Ulfbeck, C. Coath, A. N. Krot and M. Bizzaro, *Science*, 2009, **324**, 374–376.

7 R. C. J. Steele, C. D. Coath, M. Regelous, S. Russell and T. Elliott, *Astrophys. J.*, 2012, **758**, 59–80.

8 A. Trinquier, J. L. Birck, C. J. Allègre, C. Göpel and D. Ulfbeck, *Geochim. Cosmochim. Acta*, 2008, **72**, 5146–5163.

9 M. K. Weisberg, T. J. McCoy and A. N. Krot, in *Meteorites and the early solar system II*, 2006, vol. 19.

10 C. Burkhardt, T. Kleine, F. Oberli, A. Pack, B. Bourdon and R. Wieler, *Earth Planet. Sci. Lett.*, 2011, **312**, 390–400.

11 J. H. Chen, D. A. Papanastassiou and G. J. Wasserburg, *Geochim. Cosmochim. Acta*, 2010, **74**, 3851–3862.

12 M. Fischer-Gödde, C. Burkhardt, T. S. Kruijer and T. Kleine, *Geochim. Cosmochim. Acta*, 2015, **168**, 151–171.

13 T. S. Kruijer, M. Fischer-Gödde, T. Kleine, P. Sprung, I. Leya and R. Wieler, *Earth Planet. Sci. Lett.*, 2013, **361**, 162–172.

14 Q. Liping, D. Nicolas, W. Meenakshi, M. Agnès, G. Roberto, E. J. Philip and B. Claudia, *Astrophys. J.*, 2008, **674**, 1234–1241.

15 M. Regelous, T. Elliott and C. D. Coath, *Earth Planet. Sci. Lett.*, 2008, **272**, 330–338.

16 B. Mayer, N. Wittig, M. Humayun and I. Leya, *Astrophys. J.*, 2015, **809**, 180–187.

17 N. Wittig, M. Humayun, A. D. Brandon, S. Huang and I. Leya, *Earth Planet. Sci. Lett.*, 2013, **361**, 152–161.

18 S. Bisterzo, R. Gallino, O. Straniero, S. Cristallo and F. Käppeler, *Mon. Not. R. Astron. Soc.*, 2011, **418**, 284–319.

19 I. Leya and J. Masarik, *Meteorit. Planet. Sci.*, 2013, **48**, 665–685.

20 M. Schönbächler, R. W. Carlson, M. F. Horan, T. D. Mock and E. H. Hauri, *Geochim. Cosmochim. Acta*, 2008, **72**, 5330–5341.

21 K. J. Theis, M. Schönbächler, G. K. Benedix, M. Rehkämper, R. Andreasen and C. Davies, *Earth Planet. Sci. Lett.*, 2013, **361**, 402–411.

22 M. Matthes, M. Fischer-Gödde, T. S. Kruijer, I. Leya and T. Kleine, *Geochim. Cosmochim. Acta*, 2015, **169**, 45–62.

23 C.-L. Chou, *9th Lunar and Planetary Science Conference*, Houston, 1978.

24 R. J. Walker, *Chem. Erde*, 2009, **69**, 101–125.

25 K. Righter, M. Humayun and L. Danielson, *Nat. Geosci.*, 2008, **1**, 321–323.

26 M. Hoashi, R. R. Brooks and R. D. Reeves, *Chem. Geol.*, 1993, **106**, 207–218.

27 Z. Chu, Y. Yan, Z. Chen, J. Guo, Y. Yang, C. Li and Y. Zhang, *Geostand. Geoanal. Res.*, 2015, **39**, 151–169.

28 M. Rehkämper and A. N. Halliday, *Talanta*, 1997, **44**, 663–672.

29 A. Hunt, M. Ek and M. Schönbächler, *Geostand. Geoanal. Res.*, submitted.

30 M. Schönbächler and M. A. Fehr, in *Treatise on Geochemistry*, ed. K. K. Turekian, Elsevier, Oxford, 2nd edn, 2014, vol. 15.7, pp. 123–146.

31 J. P. Faris, *Anal. Chem.*, 1960, **32**, 520–522.

32 K. J. R. Rosman and J. R. D. Laeter, *Geochim. Cosmochim. Acta*, 1974, **38**, 1665–1677.

33 W. A. Russell, D. A. Papanastassiou and T. A. Tombrello, *Geochim. Cosmochim. Acta*, 1978, **42**, 1075–1090.

34 W. Kelly and G. Wasserburg, *Geophys. Res. Lett.*, 1978, **5**, 1079–1082.

35 K. J. R. Rosman, I. L. Barnes, L. J. Moore and J. W. Gramlich, *Geochem. J.*, 1980, **14**, 269–277.

36 M. Huang and A. Masuda, *Anal. Chem.*, 1997, **69**, 1135–1139.

37 M. Berglund and M. E. Wieser, *Pure Appl. Chem.*, 2011, **83**, 397–410.

38 M. Shima, C. E. Rees and H. G. Thode, *Can. J. Phys.*, 1978, **56**, 1333–1339.

39 A. C. Hunt, P. M. Reger, D. L. Cook, M. Ek and M. Schönbächler, *47th Lunar and Planetary Science Conference*, Houston, 2016.